VIIRS Reflective Solar Bands On-Orbit Calibration Five-Year Update: Extension and Improvements

Junqiang Sun[1,2] and Menghua Wang[1]

[1]NOAA/NESDIS Center for Satellite Applications and Research, College Park, MD 20740, USA
[2]Global Science and Technology, Inc., 7855 Walker Drive, Suite 200, Greenbelt, MD 20770, USA

ABSTRACT

The Suomi National Polar-orbiting Partnership (SNPP) Visible Infrared Imaging Radiometer Suite (VIIRS) has been on-orbit for almost five years. VIIRS has 22 spectral bands, among which fourteen are reflective solar bands (RSB) covering a spectral range from 0.410 to 2.25 μm. The SNPP VIIRS RSB have performed very well since launch. The radiometric calibration for the RSB has also reached a mature stage after almost five years since its launch. Numerous improvements have been made in the standard RSB calibration methodology. Additionally, a hybrid calibration method, which takes the advantages of both solar diffuser calibration and lunar calibration and avoids the drawbacks of the two methods, successfully finalizes the highly accurate calibration for VIIRS RSB. The successfully calibrated RSB data record significantly impacts the ocean color products, whose stringent requirements are especially sensitive to calibration accuracy, and helps the ocean color products to reach maturity and high quality. Nevertheless, there are still many challenge issues to be investigated for further improvements of the VIIRS sensor data records (SDR). In this presentation, the robust results of the RSB calibrations and the ocean product performance will be presented. The reprocessed SDR is now in more science tests, in addition to the ocean science tests already completed one year ago, readying to be the mission-long operational SDR

Keywords: SNPP, VIIRS, RSB, Radiometric Calibration, Solar Diffuser, Solar Diffuser Stability Monitor, Moon

1. INTRODUCTION

The Visible Infrared Imaging Radiometer Suite (VIIRS)[1,2] is one of five instruments on-board the Suomi National Polar-orbiting Partenership (SNPP) satellite successfully launched on October 28, 2011. VIIRS has 22 spectral bands covering a spectral range from 0.410 to 12.013 μm. Among them, fourteen are Reflective Solar Bands (RSB), seven are thermal emissive bands (TEB), and one is a day/night band (DNB). The VIIRS RSB are calibrated on orbit with an on-board Solar Diffuser (SD)[3-6] with its degradation tracked by a Solar Diffuser Stability Monitor (SDSM).[7-9] The VIIRS RSB on-orbit changes are also monitored with scheduled monthly lunar observations through the instrument's Space View (SV).[10,11] Fig. 1 is a schematic diagram for VIIRS instrument and on board calibrators. Table 1 shows the wavelengths of the RSB and the wavelengths at which the SD degradation is tracked by the SDSM detectors. For VIIRS, the Angle of Incidence (AOI) of the SV is exactly the same as that of the SD. This is an important design element that allows the lunar observation to track the VIIRS RSB gain change at the same AOI as the SD calibration. In principle, the two should provide the same on-orbit gain variation for all RSB and this has proven to be a decisive factor in the eventual robust result.

The robust RSB calibration is achieved component by component.[12,13] The bidirectional reflectance factor (BRF) of the SD toward the rotation telescope assembly and the RSB, the vignetting function (VF) characterizing the transmission function of the attenuation screen in front of the SD port,[14] the selection of the "sweet spot" for the correct fully-illuminated scans during calibration events, the degradation factor of the SD reflectance or so called H-factors,[9] and finally the RSB calibration coefficients, or F-factors,5 are among the key components rigorously examined. A new successful development is the "Hybrid-method"-derived RSB calibration coefficients to mitigate the known inherent growing RSB calibration error that has been observed for numerous years.[13] The result of the lunar calibration, as mentioned above, is the decisive factor in resetting the correct calibration baseline to avert the erroneous result coming from the standard calibration methodology base on the SD. The Hybrid-based and the improved F-factors lead to the highly accurate Sensor Data Record (SDR) crucial for VIIRS environmental data records (EDR) ocean color products.[12,13] We have re-analyzed and re-processed all data of the SD and SDSM observations and derived the H- and

Earth Observing Systems XXI, edited by James J. Butler, Xiaoxiong (Jack) Xiong, Xingfa Gu, Proc. of SPIE
Vol. 9972, 99721B · © 2016 SPIE · CCC code: 0277-786X/16/$18 · doi: 10.1117/12.2236997

F-factors for the entire mission of the SNPP VIIRS. In addition, the lunar calibration has become mainstream for the RSB calibration of SNPP VIIRS. It is appropriate to mention here that careful schedule planning, determination of the correct phase angle range, correction to the lunar view geometry effect, etc, all have been properly carried out to achieve the robust result in lunar-based calibration that has become critical for the final overall RSB calibration accuracy.

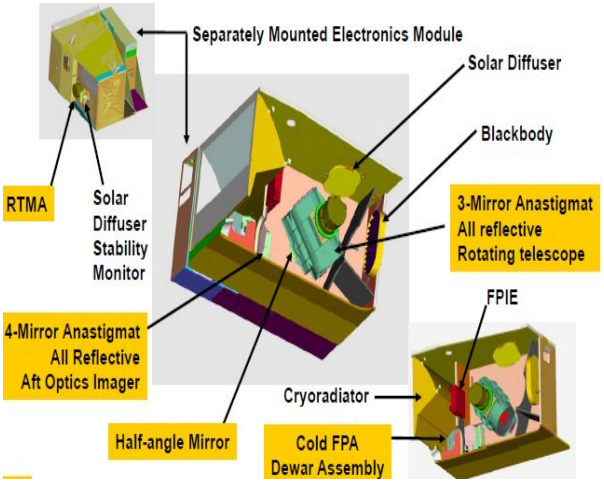

Fig. 1. VIIRS instrument and its on-board calibrators.

Table 1. VIIRS RSB and SDSM Specification

VIIRS Bands	CW* (nm)	Band Gain	SDSM Detector	CW (nm)
M1	410	DG	D1	412
M2	443	DG	D2	450
M3	486	DG	D3	488
M4	551	DG	D4	555
I1	640	SG	NA	NA
M5	671	DG	D5	672
M6	745	SG	D6	746
M7, I2	862	DG, SG	D7	865
NA	NA	N	D8	935
M8	1238	SG	NA	NA
M9	1378	SG	NA	NA
M10, I3	1610	SG, SG	NA	NA
M11	2250	SG	NA	NA

*CW: Center Wavelength; DG: Dual Gain; SG: Singla Gain

In this paper, we review the standard SDSM and SD calibration algorithms of the VIIRS RSB, follow by the description ot the lunar calibration algorithms and finally the Hybrid-calibration algorithm that eventually provided the long-term stable results. A brief presentation on the result of the ocean color science tests showing significant improvement is given.

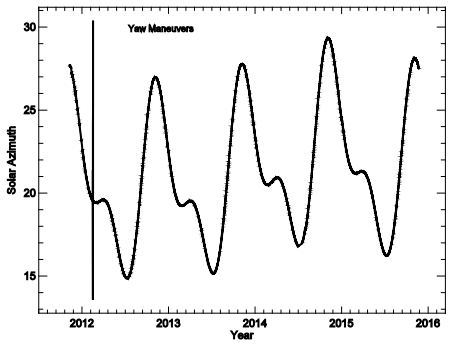

Fig. 2. "Sweet spot" for the SDSM SD and the sun view.

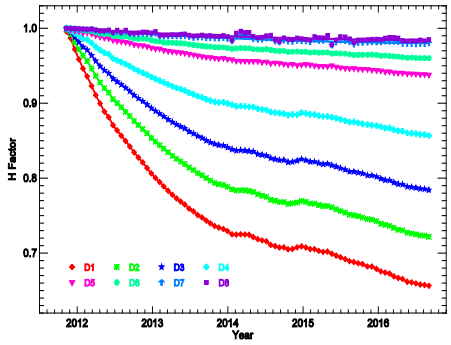

Fig. 3. SD degradation derived from SDSM calibration.

2. SDSM CALIBRATION

The SNPP VIIRS SDSM is a ratio radiometer which consists of a spherical integrating sphere (SIS) with a single input aperture and eight filtered detectors. The center wavelengths of the eight SDSM detectors are listed in Table 1. The SDSM views the SD, Sun, and the dark scene inside the SDSM. The dark scene response provides the background response of the SDSM. In the SDSM calibration methodology, a linear approximation is applied to establish the relationship between the radiance of the incident sunlight at the center wavelength of a SDSM detector and the background-subtracted digital count from the detector. Both the SD, through the SD port, and the SDSM entrance aperture, through the SD sun-view port, are fully illuminated during a short window of time when the satellite

approaches the South Pole from the night side of the Earth. Only the SDSM responses to the SD with the view spot being fully illuminated and those to the sun view with the SDSM aperture fully illuminated can be used to derive the SD degradation. The SD degradation at the center wavelength of the SDSM detector can be tracked by the ratio of the detector's SD view response to its sun view response. The effects of view geometry in the two responses are corrected with the prelaunch measured and on-orbit validated BRF of the SD and VFs of the SD as well as other incident angle dependent effect and Earth-Sun distance effect. Figure 2 shows the solar azimuth angle for entire mission including the coverage range of the angle in the yaw measurements.[15] It is clearly seen that the solar azimuth angle is fully within the coverage range of the yaw measurements and then the BRF and VF validated by the yaw measurements should work properly for the entire mission. To reduce the random noise, only the scans in the selected "sweet spots" in the fully illumination window for the two views are used to calculate the SD degradation.

The on-orbit SD degradations derived from SDSM measurements at the wavelengths of the SDSM detectors are shown in Fig. 3 in symbols. The first set of SDSM measurements was made on November 8, 2011 when the SNPP VIIRS was turned on after 11 days on orbit. The nadir door was opened on November 21, 2011. The SD started to degrade before the nadir door open due to the solar illumination through the SD door and the SD degraded much faster after the opening of the nadir door because of extra solar illumination coming from the sunlight scattered from the earth surface. Since the SD door is always open, the SD should start to degrade at the very first day launched, October 28, 2011, even though the instrument was not yet turned on. The SD degradation shows the expected result that the degree of degradation is greater at lower wavelength. In the past five years since the VIIRS has gone on-orbit, the SD has degraded about 34.3%, 27.7%, 21.6%, 14.2%, 6.1%, 4.0%, 2.0%, and 1.7% at wavelengths of 412, 450, 488, 555, 672, 746, 865, and 935 nm, respectively.

The SD degrades with time in first two years but with changing degradation rate as expected. Unexpected performance of the SD reflectance occurred in the year 2014 and the SD degrade smoothly since then in the last two years. The unexpected pattern of the SD reflectance in 2014 has been identified as a real SD reflectance change from results in the calculated RSB calibration coefficients, the F-factors, using the SD calibration and the VIIRS ocean color products. The results in Fig. 3 demonstrate that the SD degradation can be accurately tracked by the SDSM calibration. However, it is carefully noted that the SDSM calibration catches the SD degradation for the outgoing direction toward the SDSM view direction but not in the direction toward the RSB. The standard methodology assumes that the SD degrades uniformly with the incident and outgoing directions, and the SD degradation derived from the SDSM calibration is applied in the SD calibration to derive the RSB calibration coefficients.

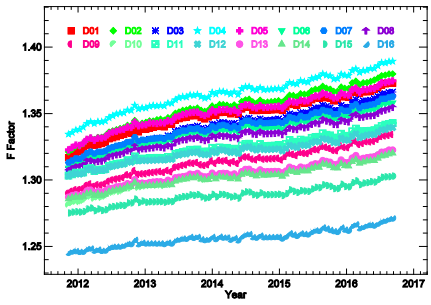

Fig. 4. VIIRS band M1high gain HAM 1 F factors.

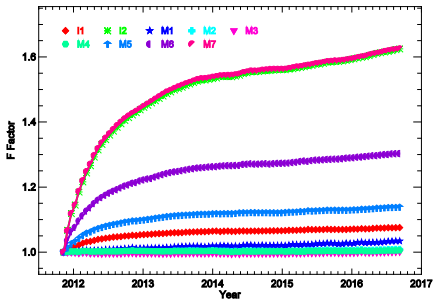

Fig. 5. VIIRS detector averaged high gain HAM 1 F factors.

3. SD CALIBRATION

The VIIRS SD shown is made of Spectralon® and is used to calibrate the RSB on-orbit. The center wavelengths of the RSB are listed in Table 1. The details will not be presented here, but one crucial point is that the SD degrades uniformly with respect to the outgoing direction, hence that the SDSM-measured H-factor can be used as a valid substitute for the H-factor toward the RSB view. By comparing the measured SD radiance calculated with the quadratic form of the instrument response and the calculated SD radiance, the calibration coefficients, F-factors, for a RSB from each SD

observation are derived. However, it has been shown that this SD degradation uniformity condition is not true, thus creating a serious problem within the standard calibration methodology. The Hybrid-method to be presented later provides a fix to this issue.

SNPP VIIRS SD calibration is performed in every orbit generating about 14 events every. The RSB calibration coefficients, SD F-factors, derived from the SD calibration for VIIRS band M1 high gain HAM 1 are shown in Fig. 4. The F-factors in Fig. 4 are measured values from each individual measurement without using any smooth or average algorithm. The results show increase with time, are clearly detector dependent, and are very smooth with random fluctuations on the level of ~±0.1% in the F-factors. Considering that the specification for the RSB calibration is 2% and the expectation for the stability of the F-factors from the ocean color applications, which have much higher requirements for the accuracy of the RSB calibration than those from other science disciplines, is about 0.2%, the F-factors in Fig. 4 are remarkably stable. The detector averaged high gain HAM 1 F-factors for visible and near infrared RSB are displayed in Fig. 5. They are strongly band or wavelength dependent. The largest increase occurs at near infrared band I2 and M7, both of which have the same wavelength of 862 nm, while the increases for the short wavelength bands are much smaller. This is very different from MODIS RSB for which the largest degradation occurs at short wavelength bands. The F-factors of bands I2 and M7 have increased about 63% since launch on October 28, 2014, while the increases for bands M1, M2, and M3 are less than 3.5%, respectively. Band M3 has the least increase. For VIIRS RSB, there are two main competing mechanisms for the change. One is degradation of the HAM, which may degrade more at short wavelengths, while the other is the degradation of the RTA, which degrades much faster at the NIR range. The SD calibration can provide very stable and smooth calibration coefficients for the RSB, except that the assumption that the SD degrades uniformly, as mentioned to be a key point for the standard calibration procedure, is not true.

4. LUNAR CALIBRATION

It is well known that the reflectance of the lunar surface is very stable in visible and near infrared spectral regions. It can then be used as a reference to calibrate the RSB of a remote sensor. However, the lunar surface is not smooth and the radiance of the lunar view cannot be directly used to derive the calibration coefficients. We have to use the lunar irradiance instead of the radiance to calibrate the RSB. The lunar radiance strongly depends on the view geometry, especially the lunar phase angle. To reduce the uncertainty of the correction of the lunar view geometry effect, it is better to minimize the differences of the lunar view geometries for a given sensor. To get the similar view geometries and also to increase the opportunity of the lunar observations, instrument roll maneuvers are usually applied and a planning tool is needed to plan the lunar observations. The SNPP VIIRS has been scheduled to view the Moon monthly in nine months every year since launch through its SV port. Every year, there are three months in summer, during which the instrument cannot view the Moon with the constraint of the roll maneuver.

Even though the differences of the lunar view geometries can be minimize with good planning, there are still differences among the lunar view geometries. Their impacts on the lunar irradiance then need to be corrected in order to get accurate calibration coefficients from the lunar observations. A model, called ROLO model,[16,17] have been developed to predict the lunar irradiance for any given lunar view geometry and the predicted lunar irradiance by the lunar model can be used to account for the geometric effect. By the taking the ratio of the ROLO model prediction and the lunar irradiance calculated with the prelaunch calibration coefficients, the SNPP VIIRS RSB calibration coefficients can be derived from a lunar observation. The absolute uncertainty of the ROLO model can be as large as 5% for short-wavelength bands and the uncertainty is even larger for NIR bands. Then the lunar calibration cannot provide the accurate absolute calibration coefficients but only relative changes since the first lunar observation. The relative uncertainty of the irradiance predicted by the ROLO model over the entire view geometry is about 1%, which induces seasonal oscillations in the derived calibration coefficients. To remove the oscillations and improve the accuracy of the calibration coefficients, we have developed an extra correction based on the lunar librations to reduce the uncertainty of the predicted lunar radiance. Since the AOI of the SD and the SV is the same, the lunar and the SD/SDSM calibration track the on-orbit gain change at the same AOI and, then, should provide the same calibration coefficients changes when they are normalized at any given time.

The F-factors, lunar F-factors, derived for SNPP VIIRS visible and near infrared bands from the scheduled lunar observations are shown in Fig. 6 in symbols. The three months of the year when moon cannot be seen are reflected as data gaps. For comparison, the corresponding F-factors derived from the SD/SDSM calibration are also drawn in the

plot as lines. The F-factors are normalized at the time of the first scheduled lunar observation for each band. From the plot, it can be seen that the F-factors from the two calibrations agree with each other reasonably well for most bands but with some differences between the two sets of F-factors. To clearly see the differences, Figure7 shows the F-factors derived from the SD/SDSM calibration and the lunar calibration only for bands M1-M4 on a smaller scale. It is seen clearly that the differences between the F-factors derived from the SD/SDSM calibration and those from the lunar calibration increase with time and the largest difference occurs in band M4, which is about 1.5%. From both Figs. 6 and 7, it is seen that the lunar SD F-factors change with time smoothly and are very stable (with noises being smaller than 0.2%). Figure 8 shows the ratios of the lunar F-factors and the SD F-factors. It is clearly shown that the ratios are band dependent and they all increase with time. Bands I1, M3, and M4 have largest ratios among all the bands. One of the root causes of the differences between the SD/SDSM calibration and the lunar calibration for SNPP VIIRS is known to be the non-uniformity of the SD degradation with respect to the incident and outgoing directions. This can explain the differences between the two sets of the F-factors for the short-wavelength bands but for bands I1, M3, and M4. For these three bands and other long-wavelength band, the full causes are still unknown.

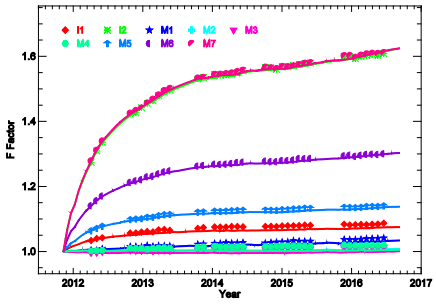

Figure 6. SNPP VIIRS visible bands lunar irradiance.

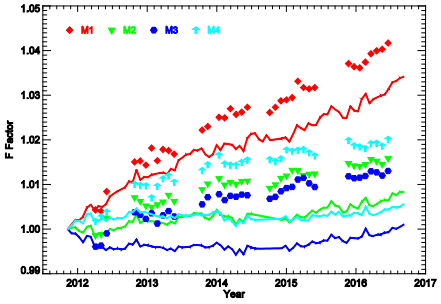

Figure 7. SNPP VIIRS RSB F-factors and lunar F-factors.

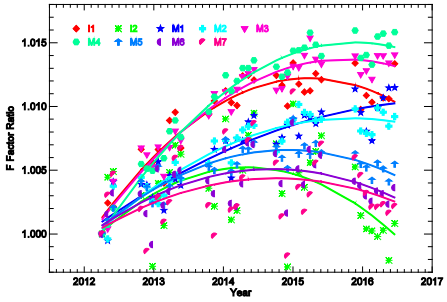

Fig. 8. Lunar and SD F-factors ratios.

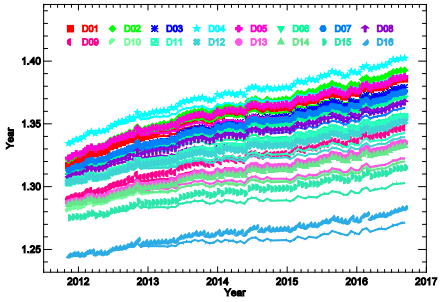

Fig.9. Hybrid F-factors (symbols) and SD F-factors (lines) for the band M1.

5. HYBRID CALIBRATION

SD/SDSM or lunar calibration alone has its advantages and disadvantages. Lunar calibration provides more accurate and reliable long-term VIIRS RSB on-orbit changes of the RSB F-factors but is less frequent, only about nine times each

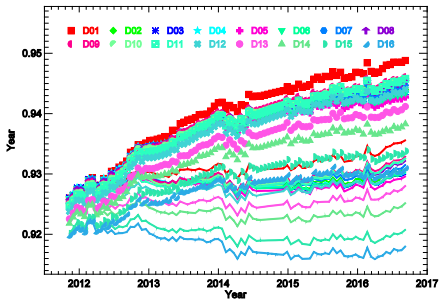

Fig. 10. Hybrid F-factors (symbols) and SD F-factors (lines) for the band M4.

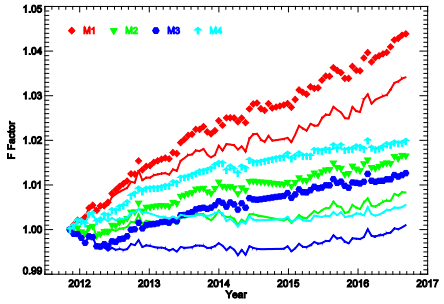

Fig. 11. Band averaged hybrid F-factors (symbols) and band averaged SD F-factors (lines).

year. On the other hand, the SD/SDSM calibration can provide VIIRS on-orbit changes of the RSB F-factors for each orbit and is smooth and stable in the short time frame although the derived F-factors may long-term bias due to degradation non-uniformity effect[18] and possibly other effects. A hybrid approach has been proposed and applied to combine the two sets of F-factors by using the lunar F-factors as the long-term baseline and the SD F-factors for the short-term gain variation.[1]

The SD F-factors and the hybrid F-factors for band M1 high gain HAM 1 are displayed in Figure 9, in solid lines for SD F-factors and in symbols for hybrid F-factors. Both sets of the F-factors are smooth and stable. Figure 10 shows the same results for band M4. Similarly, the both sets of F-factors are smooth and stable while the hybrid F-factors have more reasonable trend. For a few detectors at high detector numbers, the SD F-factors increase in very early mission as expected but started to decrease after about one year. The decrease of the F-factors means the increase in gain, which is unlikely true for a visible band. Unlike the SD F-factors, the hybrid F-factors for all detectors of the band smoothly increase with time for the entire mission. The continuous increase of the hybrid F-factors matches the expectation of the band on-orbit performance. Figure 11 displays the band-averaged hybrid F-factors and SD F-factors for short wavelength bands M1 – M4. As expected, the hybrid F-factors are larger than the SD F-factors and the differences between the two sets of F-factors increase with time. It is also seen that the differences between the two sets of F-factors for M4 are larger than those for the other three bands. This is consistent with the ratios of the lunar and SD F-factors displayed in Fig. 8. The hybrid approach is not applied to the time period before April 2012 due to the inaccuracy of the lunar F-factors induced by the partial observations of the lunar surface [10, 11].

6. SDR and Ocean Color EDR Improvements

The reprocessed SDR, with the full RSB calibration improvements presented in this paper incorporated, has been generated for the application to the ocean color EDR products. The main ocean color EDR products are the normalized water-leaving radiance spectra, $nL_w(\lambda)$, which is approximately the radiance that would exit the ocean in the absence of atmosphere and with Sun at the zenith.[19] It is wavelength dependent and can be computed for the wavelength of each of the instrument's ocean bands designed for ocean color applications. From the radiances at the wavelengths of the ocean bands, ocean optical, biological, and biogeochemical properties can be derived. Since the atmosphere and ocean surface radiances contribute about more than 90% in the TOA radiance in visible wavelength range, water-leaving radiance only contributes about 10% or less to the top of atmosphere radiance (TOA).[20] Since the atmosphere and ocean surface contributions to the TOA radiances (i.e., atmospheric correction) are simulated using a theoretical model, all instrument calibration errors are passed on to satellite-derived water-leaving radiance spectra.[19,20] Thus the percentage of the uncertainty in the SDR radiance (or calibration uncertainty) will be amplified approximately by an order of magnitude in the normalized water-leaving radiance (or ocean color EDR products)[19-21] . Therefore, the radiometric accuracy of the RSBs is critical to the quality of ocean color products [25]. All other ocean color EDR products are derived from the

normalized water-leaving radiance. Chlorophyll-*a* concentration, *Chl-a*, is an estimate of the phytoplankton biomass and can be derived from the $nL_w(\lambda)$ at the wavelengths of 443 (or 486) and 551 nm. For VIIRS, they correspond to the centre wavelengths of bands M2 (or M3) and M4, respectively.

The NOAA Ocean Color Team has developed a global near-real-time VIIRS ocean color data processing system, which automatically downloads global VIIRS RDR (Level-0), SDR (Level-1B), and ancillary data in near real-time, and then processes them into ocean color EDR (Level-2) data [19] using the NOAA Multi-Sensor Level-1 to Level-2 (NOAA-MSL12) software package.[20,22,23] The team also routinely generates the global Level-3 binned products (daily, 8-day, monthly, and climatology) for evaluation purpose (http://www.star.nesdis.noaa.gov/sod/mecb/color/).[24,25] Using the system, the NOAA Ocean Color team has been routinely processing and evaluating VIIRS ocean color products from the start of the VIIRS mission using the IDPS SDR products. The team has also reprocessed ocean color EDR using the SDR processed with the hybrid F-factors. The team also routinely processes the SDR using the hybrid F-factors[12,13] and then produce the ocean color EDR with high data quality and accuracy using the improved SDR for the forward daily processing. The previously mentioned ratio-approach method, which reduces the computational effort at least by two magnitudes,[26] has been utilized since December, 2015 in the routine process. The method can be directly applied in ocean color EDR processing to reduce the computational effort and to avert the huge disk storage need for improved SDR. In fact, the NOAA Ocean Color Team uses the latter approach for VIIRS ocean color EDR reprocessing and the forward daily processing with scientific quality using the hybrid F-factors.

The preliminary evaluation of the reprocessed ocean color EDR using the SDR generated with the hybrid F-factors has been reported in our previous papers.[12,13] The detailed evaluation of the improvements of new hybrid LUTs on the ocean color products, as well as the improvements of the ocean color algorithms, have been reported in various conferences and will be documented elsewhere. Here we briefly show the improvements of the hybrid F-factors on the VIIRS ocean color products. Figures 12 shows the time series of VIIRS-derived $nL_w(\lambda)$ at wavelength 551 nm (M4) over the Hawaii region (oligotrophic waters). The $nL_w(\lambda)$ spectra derived with the IDPS SDR processed with standard operational F-factors are represented by solid diamonds. The $nL_w(\lambda)$ derived using the SDR produced with our hybrid F-factors at the are shown by solid squares. The figure shows that $nL_w(\lambda)$ data derived with the IDPS SDR have a large anomaly before April 20, 2012 and a long-term drift. The newly derived $nL_w(\lambda)$ spectra with the hybrid F-factors are much improved and the long-term drifts are significantly reduced. This is also true for all other visible bands. The trend from the Marine Optical Buoy (MOBY) data, the direct in-situ measurements of $nL_w(\lambda)$ using a system of buoys,[27,28] are also shown in Fig. 12 (in solid triangles). The comparison with the MOBY result further confirms that the SDR using hybrid F-factors significantly elevates the accuracy of the ocean color products. Figure 13 shows VIIRS *Chl-a* derived from the newly reprocessed SDR with the hybrid F-factors and from the IDPS SDR in the ocean global oligotropic waters.

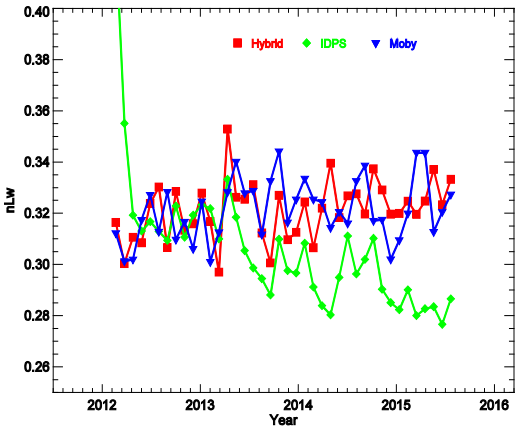

Fig. 12. Ocean $nL_w(\lambda)$ trending for the band M4 along with MOBY in-situ data.

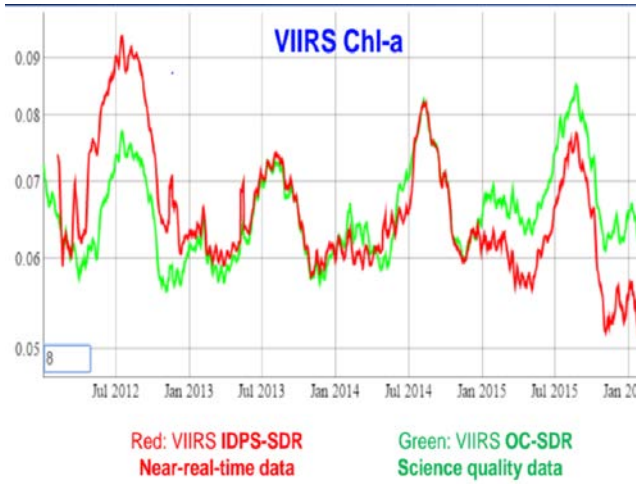

Fig. 13. Ocean Global Oligotropic waters *Chl-a* trending.

Forward delivery of science quality ocean color products is already in operation. As of September 2016, the reprocessed SDR is going through land and atmospheric science tests, to be completed before the end of the year, before becoming the mission-long operational SDR.

7. SUMMARY

We have presented the on-orbit RSB calibration for VIIRS and the updated the five-year results. The improvements successfully corrected each respective issue in RSB calibration. The overall RSB calibration methodology, with the Hybrid-method mitigation added, is working as expected. The H- and the F-factors have been calibrated to achieve a high stability on the level of 0.2%, with minimal noise and numerical artifacts. Most importantly the long-term drifts that are present in other data versions, in both SDR and EDR, due to the inherent RSB calibration bias, has been removed. The five-year update demonstrates that the efforts by the NOAA Ocean Color Team have succeeded in generating robust RSB calibration result, leading to accurate SDR and eventual ocean color science products. The path for the reprocessed SDR to become the official operational products is currently going through land and atmosphere science tests.

ACKNOWLEDGEMENTS

The work was supported by the Joint Polar Satellite System (JPSS) funding. We would like to thank Mike Chu for helpful suggestions and support, and other members of the NOAA Ocean Color Team for their support. The views, opinions, and findings contained in this paper are those of the authors and should not be construed as an official NOAA or U.S. Government position, policy, or decision.

REFERENCES

1. C. Cao, F. Deluccia, X. Xiong, R. Wolfe, and F. Weng, “Early on-orbit performance of the Visible Infrared Imaging Radiometer Suite (VIIRS) onboard the Suomi National Polar-orbiting Partnership (S-NPP) satellite,” IEEE Trans. Geosci. Remote Sens., 52, 1142–1156 (2014).
2. C. Cao, F. Deluccia, X. Xiong, R. Wolfe, and F. Weng, “Early on-orbit performance of the Visible Infrared Imaging Radiometer Suite (VIIRS) onboard the Suomi National Polar-orbiting Partnership (S-NPP) satellite,” IEEE Trans. Geosci. Remote Sens., 52, 1142–1156 (2014).
3. X. Xiong, J. Butler, K. Chiang, B. Efremova, J. Fulbright, N. Lei, J. McIntire, H. Oudrari, J. Sun, Z. Wang, and A. Wu, “VIIRS on-orbit calibration methodology and performance,” J. Geophys. Res. Atmos., 119, 5065–5078 (2014).
4. N. Lei, Z. Wang, J. Fulbright, S. Lee, J. McIntire, K. Chiang, and X. Xiong, “Initial on-orbit radiometric calibration of the Suomi NPP VIIRS reflective solar bands,” Proc. SPIE, 8510, 851018 (2012).
5. J. C. Cardema, K. Rausch, N. Lei, D. I. Moyer, and F. DeLuccia, “Operational calibration of VIIRS reflective solar band sensor data records,” Proc. SPIE, 8510, 851019 (2012).
6. J. Sun and M. Wang, “On-orbit calibration of Visible Infrared Imaging Radiometer Suite reflective solar bands and its challenges using a solar diffuser,” *Appl. Opt.*, 54, 7210-7223 (2015).
7. R. E. Eplee, Jr., K. R. Turpie, G. Meister, F. S. Patt, B. A. Franz, S. W. Bailey, “On-orbit calibration of the Suomi National Polar-Orbiting Partnership Visible Infrared Imaging Radiometer Suite for ocean color applications,” *Appl. Opt.* 54, 1984-2006 (2015).
8. J. Fulbright, N. Lei, K. Chiang, and X. Xiong, “Characterization and performance of the Suomi-NPP VIIRS solar diffuser stability monitor,” Proc. SPIE, 8510, 851015 (2014).
9. E. Hass, D. Moyer, F. DeLuccia, K. Rausch, and J. Fulbright, “VIIRS solar diffuser bidirectional reflectance distribution function (BRDF) degradation factor operational trending and update,” Proc. SPIE, 8510, 851016 (2012).
10. J. Sun and M. Wang, “Visible infrared image radiometer suite solar diffuser calibration and its challenges using solar diffuser stability monitor,” *Appl. Opt*., 53, 8571-8584 (2014).
11. J. Sun, X. Xiong, and J. Butler, “NPP VIIRS on-orbit calibration and characterization using the Moon,” *Proc. SPIE*, vol. vol. 8510, pp. 85101I, doi: 10.1117/12.939933, 2012.

12. X. Xiong, J. Sun, J. Fulbright, Z. Wang, and J. Butler, "Lunar Calibration and Performance for S-NPP VIIRS Reflective Solar Bands", submitted to *IEEE Trans. Geosci. Remote Sensing.*, 54, 1052-1061 (2016).
13. . Sun and M. Wang, "VIIRS Reflective Solar Bands Calibration Progress and Its Impact on Ocean Color Products," *Remote Sensing*, 8, 194, (2016).
14. J. Sun and M. Wang, "Radiometric calibration of the Visible Infrared Imaging Radiometer Suite reflective solar bands with robust characterizations and hybrid calibration coefficients", *Appl. Opt*., 54, 9331-9342 (2015).
15. J. Sun and M. Wang, "On-orbit characterization of the VIIRS solar diffuser and solar diffuser screen," Appl. Opt., 54, 236-252 (2015).
16. J. Sun and X. Xiong, "Solar and lunar observation planning for Earth-observing sensor", *Proc. SPIE*, 8176, 817610, (2011).
17. Hugh H. Kieffer and Thomas C. Stone, "The Spectral Irradiance of the Moon", *Astronom. J.* 129, 2887-2901 (2005).
18. T.C. Stone and H.H. Kieffer, "Assessment of Uncertainty in ROLO Lunar Irradiance for On-orbit Calibration", *Proc. SPIE* 5542, 300-310 (2004).
19. Sun, J., M. Chu, and M. Wang, "Degradation nonuniformity in the solar diffuser bidiretional reflectance distribution function", *Appl. Opt.*, 55, 6001-6016 (2016).
20. H. R. Gordon, and M. Wang, "Retrieval of water-leaving radiance and aerosol optical thickness over the oceans with SeaWiFS: A preliminary algorithm," Appl. Opt., 33, 443–452 (1994).
21. M. Wang and B. A. Franz, "Comparing the ocean color measurements between MOS and SeaWiFS: A vicarious intercalibration approach for MOS," IEEE Trans. Geosci. Remote Sens. 38, 184–197 (2000).
22. M. Wang, "Remote sensing of the ocean contributions from ultraviolet to near-infrared using the shortwave infrared bands: simulations," Appl. Opt., 46, 1535–1547 (2007).
23. M. Wang, A. Isaacman, B. A. Franz, and C. R. McClain, "Ocean color optical property data derived from the Japanese Ocean Color and Temperature Scanner and the French Polarization and Directionality of the Earth's Reflectances: A comparison study," Appl. Opt. 41, 974–990 (2002).
24. IOCCG, "Mission Requirements for Future Ocean-Colour Sensors," C. R. McClain and G. Meister (Eds.), *Reports of International Ocean-Colour Coordinating Group*, No. 13 (IOCCG, Dartmouth, Canada, 2012).
25. M. Wang, W. Shi, and J. Tang, "Water property monitoring and assessment for China's inland Lake Taihu from MODIS-Aqua measurements," *Remote Sens. Environ.*, 115, 841–845, 2011.
26. M. Wang, X. Liu, L. Tan, L. Jiang, S. Son, W. Shi, K. Rausch, and K. Voss, "Impact of VIIRS SDR performance on ocean color products," J. Geophys. Res. Atmos., 118, 10347–10360 (2013).
27. J. Sun, M. Wang, L. Tan, L. Jiang, "An Efficient Approach for VIIRS RDR to SDR Data Processing", IEEE. Trans. Geosci. Remote Sens. Lett., 11, 2037-2041, 2014.
28. D. Clark, H. Gordon, K. Voss, W. Broenkow, C. Trees, et al. (1997), "Validation of atmospheric correction over the oceans," *Journal of Geophysical Research*, 102, 17209-17217 (1997).
29. D. Clark, M. Yarbrough, M. Feinholz, et al, "MOBY, a radiometric buoy for performance monitoring and vicarious calibration of satellite ocean color sensors: measurement and data analysis protocols," in J. Mueller, G. Fargion, C. McClain, *Ocean Optics Protocols for Satellite Ocean Color Sensor Validation* VI (Revision 4 ed.), Greenbelt, MD: National Aeronautics and Space Administration Goddard Space Flight Center (2003), pp. 3–34, NASA/TM-2003-211621/Rev4-Vol.VI, retrieved 2008-11-21.